Chem Soc Rev

Break junction under electrochemical gating: testbed for single-molecule electronics

Journal:	*Chemical Society Reviews*
Manuscript ID:	CS-TRV-07-2014-000242.R1
Article Type:	Tutorial Review
Date Submitted by the Author:	16-Jul-2014
Complete List of Authors:	Huang, Cancan; University of Bern, Departement of Chemistry and Biochemistry Rudnev, Alexander; University of Bern, Departement of Chemistry and Biochemistry Hong, Wenjing; University of Bern, Departement of Chemistry and Biochemistry Wandlowski, Thomas; University of Berne, Departement of Chemistry and Biochemistry

Chemical Soc Rev

RSCPublishing

TUTORIAL REVIEW

Break junction under electrochemical gating: testbed for single-molecule electronics

Cite this: DOI: 10.1039/x0xx00000x

Cancan Huang, Alexander V. Rudnev, Wenjing Hong,* Thomas Wandlowski

Received ooth January 2014,
Accepted ooth January 2014

DOI: 10.1039/x0xx00000x

www.rsc.org/

Molecular electronics aims to construct functional molecular devices at the single-molecule scale. One of the major challenges is to construct a single-molecule junction and to further manipulate the charge transport through the molecular junction. Break junction techniques, including STM break junctions and mechanically controllable break junctions are considered as testbed to investigate and control the charge transport on a single-molecule scale. Moreover, additional electrochemical gating provides a unique opportunity to manipulate the energy alignment and molecular redox processes for a single-molecule junction. In this review, we start from the technical aspects of the break junction technique, then discuss the molecular structure-conductance correlation derived from break junction studies, and, finally, emphasize electrochemical gating as a promising method for the functional molecular devices.

Key learning points:

1. Latest development on technical aspects for break junction experiments
2. Physics behind the single-molecule break junction measurements
3. Anchoring groups preferred in break junction measurements
4. Molecular design guideline obtained from break junction measurements
5. Electrochemical gating concept for a single-molecule break junction

1. Introduction

Molecular electronics aims at the construction of functional devices consisting of single molecules.[1] One of the major challenges for studies in the field of molecular electronics is to access the charge transport properties through molecules at the molecular scale. During the last decade, a number of techniques have been developed for this purpose. These technique can be basically divided to two main categories: the technique measuring molecule ensembles which contain tens to thousands of individual molecules,[2, 3] and single-molecule break junction technique focusing on creation of single-molecule junctions by dynamic fabrication of nanogaps after rupture of the metallic contact. Although junctions of molecular ensembles are practically closer to real devices, the break junction technique provides a unique platform to access the charge transport at a single-molecule scale in a highly dynamic mode. Repeating the formation-and-break junction cycles hundreds to thousands of times allows a statistical analysis of the data that overcomes the problem of data scattering due to variations in single-molecule junction configurations, and provides statistically significant information concerning charge transport properties. Thus, break junction techniques, including scanning tunneling microscope break junction (STM-BJ) and mechanically controllable break junction (MCBJ), are expected to be ideal testbeds to study the charge transport through single-molecule junctions.

The break junction approach can also be realized under electrochemical conditions to introduce the concept of "electrochemical gating" for single-molecule junctions. Electrochemical gating provides a unique opportunity to tune the energy level of molecule junctions and change molecular redox states at room temperature under well-controlled conditions. Thus, manipulation of charge transport of single molecules can be achieved.

In this review, we focus on single-molecule conductance studies at a solid-liquid interface using STM-BJ and MCBJ techniques. We review the latest developments in exploring charge transport characteristics of individual functional molecules by the BJ techniques. Additionally, we discuss the approach of electrochemical gating to manipulate charge transport on a single-molecule scale.

Department of Chemistry and Biochemistry, University of Bern
Freiestrasse 3, CH-3012 Bern, Switzerland
Email: hong@dcb.unibe.ch

2. Break junction techniques: construction of a

single-molecule junction

2.1. STM break junction

The scanning tunneling microscope (STM) technique provides an access to the electric properties of molecules adsorbed on a conductive substrate by combining the high resolution imaging with extension of spatially resolved current sensing spectroscopy (STS) to explore electric phenomena at the molecular scale. In 2003, Xu *et al*.[4] extended the application of STM to break junction (BJ) experiments based on the repeating formation/breaking of single-molecule junctions between a conductive STM tip and substrate. A typical STM-BJ cycle includes the following steps (Fig. 1): Initially, the molecules under study are adsorbed on the substrate through an anchoring group, and the STM tip is fixed over the molecular adlayer under activated feedback control of the tunneling current (Fig. 1A). Then, the feedback control is switched off and the BJ cycle (or *stretching* cycle) starts. The STM tip is driven by a piezoelectric transducer towards the substrate at constant x-y position until a pre-set upper limit of the current is reached (Fig. 1B). Typically, this limit corresponds to the formation of a metal-metal contact. Afterwards, the tip is withdrawn from the substrate at a pre-set rate. During this process, a target molecule can be trapped in the nanogap between tip and substrate (Fig. 1C). Upon further tip withdrawal, the molecular junction is ruptured, and the BJ cycle ends (Fig. 1D). A fixed bias potential between tip and substrate is set during the BJ cycle, and the current is recorded for further analysis. Repetition of the BJ cycles hundreds to thousand times provides a sufficient dataset for the subsequent statistical analysis, which is described in Section 2.3.

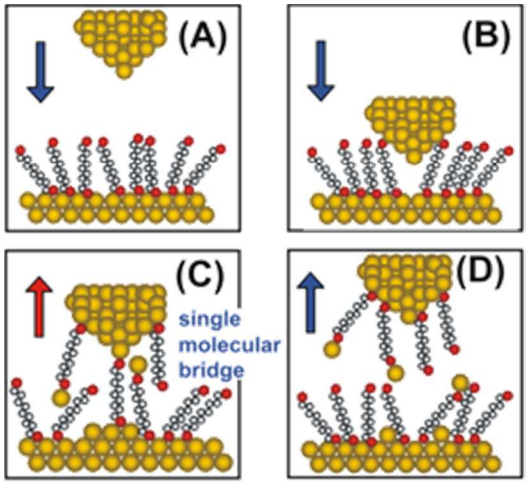

Fig. 1 Schematic of a break junction cycle in STM configuration (reprinted with permission from ref. [5] copyright © 2008 American Chemical Society).

The STM-BJ approach benefits from the well-established STM technique. Firstly, the imaging function of STM can extract structural information of the adsorbate-modified substrate surface prior to the break junction measurements. Secondly, a precise control of the contact spacing and tilt angle of the molecule with the STM tip can be achieved.[6] Force measurements of the single molecule junction can be carried out simultaneously with the conductance measurement using an atomic force microscope (AFM) and replacing the STM tip by a conductive cantilever.[7] Moreover, STM-BJ measurements can be readily performed under electrochemical conditions (discussed in Section 4).

2.2. Mechanically controllable break junction

The mechanically controllable break junction (MCBJ) technique provides another possibility to probe single-molecule junctions. During the early 1990s, Müller and Ruitenbeek *et al*.[8] introduced the MCBJ to investigate conductance quantization in metallic nanojunctions. They demonstrated that the MCBJ configuration is stable enough to establish a contact of single atoms or even a vacuum barrier of a subatomic dimension between the two electrodes. Then, Reed *et al*.[9] extended the application of the MCBJ to conductance measurements of single-molecule junctions. The target molecule, benzene-1, 4-dithiol, was assembled on two electrode surfaces. The molecular junctions were then formed during opening/closing a nanogap between the two electrodes.

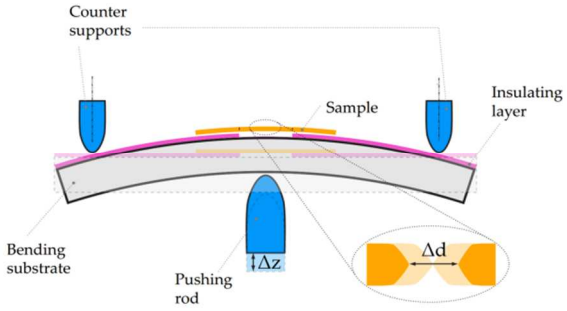

Fig. 2 Schematic of the MCBJ setup.

A typical MCBJ setup (Fig. 2) is composed of a flexible substrate with two fixed nano-spaced electrodes. This substrate is pressed from the top by two stationary rods (counter support) and a movable pushing rod underneath. A mechanical actuator, such as a piezoelectric transducer or a stepper motor, drives the pushing rod to bend/release the substrate, resulting in the opening/closing of the gap between the electrodes. Nano-spaced electrodes can be prepared by lithography or from a thin metal wire fixed to the substrate at both ends and a freely suspended middle part. In the latter case (the *notched* wire MCBJ sample), prior to the measurements, the wire is manually cut in the middle so that a thin bridge remains (monitored by an optical microscope). With the moving of the pushing rod, the thinnest part of the fixed metal wire is broken, and an adjustable nanometer-size gap is established. Using the tunneling current as feedback control signal after the complete opening of the nanogap, the pushing rod will be triggered to move down, leading to the closing of the nanogap. This process is repeated thousands of times. During the repeating cycles, the electrode contacts become atomically sharp. To perform the measurements of single molecule conductance, target molecules can be assembled on the electrodes in advance, e.g. by drop-

casting. There is another possibility, when a liquid cell is placed on top of the substrate with nano-spaced electrodes via an O-ring, and the solution of the target molecule in a non-conductive solvent is added to the cell. In the presence of the target molecules, the molecule junction can be formed during the opening/closing of the nanogap between the two electrodes similarly to the STM-BJ configuration.

Except for the lack of the imaging function, the MCBJ technique has some advantages compared to the STM-BJ. Firstly, the gap between two electrodes can be precisely controlled down to the pm-range even at room temperature. The reason for this is the low displacement ratio between the horizontal movement of the nanogap (Δd) and a vertical movement of the pushing rod (Δz) ($\sim 10^{-5}$ for lithographically fabricated samples and $\sim 10^{-2}$ for notched wire samples) and the high mechanical stability of the MCBJ. The latter is due to a relatively short distance between a single-molecule junction and the fixing points of the electrodes compared to the STM-BJ technique. Secondly, the MCBJ configuration can be easily modified, providing the opportunity for on-chip device fabrication, such as lithographically fabricated MCBJ samples using sandwich structures[10] with back gating. In addition, the combination of the MCBJ with gap-mode Raman spectroscopy provides direct access to the *in situ* monitoring of molecular junction formation simultaneously with the charge transport measurements.[11]

STM-BJ and MCBJ techniques provide complementary platforms for the formation and characterization of the single-molecule junctions. Because of the similarities in their working principles, conductance measurements of the same molecular system in a similar environment are expected to exhibit a good agreement within[12-15] and among individual laboratories.[16]

2.3. Statistical analysis to explore physics behind break junction measurements

In an idealized scenario, the current flows through a fully stretched single-molecule junction by applying a constant bias voltage. However, considering the BJ measurement as a highly dynamic process, in a more realistic scenario, there are also various possible molecular configurations with different binding geometries, when trapped in a nanogap with a certain size. Thus, it is essential to understand the nature and physical meaning behind the conductance values extracted from the break junction experiments.

Besides the variation in configurations of molecular junctions, there are still two key factors which cannot be neglected in the BJ measurements: 1) the measured conductance is obtained from the combination of a molecular conductance and a through space tunneling conductance; 2) there is a snap-back (or jump out of contact) of the two electrodes, e.g. gold electrodes. The snap-back takes place immediately after the rupture of a Au-Au contact due to its elasticity. The snap-back process is much faster than the displacement of the two electrodes upon bending the substrate. Experimental estimates give rise to ca. 0.3-0.6 nm width of the nanogap formed due to the snap-back of gold electrodes.[15]

Considering the two points, a simplified scenario of the BJ process is illustrated in Fig. 3. Different molecular configurations (panel A) and the corresponding dominant charge transport during the streching process (panel B) are described as follows: (a) Electrodes are connected, and the measured conductance G is higher than a conductance quantum G_0. The measured stretching trace is shown as solid light gray line in the panel B. (b) The electrodes form an atomic contact, which mostly contributes to the conductance ($G \sim G_0$); the molecular conductance is significantly lower than G_0. (c) The snap-back of the atomic metallic connection occurs (conductance cannot be measured). (d) An electrode-molecule-electrode junction forms, but the molecular bridge is not extended; the contribution of through space tunneling (gray line) to G still prevails over the molecular conductance contribution, which only occurs when distance between two electrode (d) is sufficiently shorter than the length of molecular junction(L) (see schematic representation in Fig. 3A).[17] (e) The electrode-molecule-electrode junction elongates, and G is mostly due to the molecular conductance. A conductance plateau is observed. (f) A fully extended molecular configuration is formed. (g) The breaking of the molecule-electrode contact with a snap-back between the molecule and one electrode. The conductance decreases sharply. (h) The tunneling channel is formed between the electrode-molecule assembly and the other electrode (gray dashed line); the conductance is measurable until it approaches the current detection limit of the setup. Numerous conductance ("stretching") traces are plotted in the 1-dimensional histogram, which may reveal a peak (or peaks) of the most probable single-molecule conductance (Figure 3B, on the right). Figure 3 illustrates that the direct tunneling between two electrodes forms a parallel conductance channel that can influence both the position and the distribution of the apparent molecular conductance extracted from histogram peaks. Based on this, Gotsmann *et al.*[17] established criteria to recognize the effect of a parallel tunneling path on the estimation of the molecular conductance from experimental data.

Due to the evolution process of molecular junction in the BJ experiments, this technique has a certain limitation. The regions marked as 1, 2, 3, 4, in Fig. 3B indicate "problematic" regions of the conductance trace. Due to the fast snap-back process, the conductance of the molecular junction within the snap-back distance cannot be resolved (region 1). There is an overlap of conductance from direct tunneling and the molecule in region 2. The snap-back upon breaking of the molecular junction (region 3) should be considered in the study of intermolecular interactions, such as π-π stacking or extended hydrogen-bonded networks. Finally, in the region 4, the conductance measurement is limited by the sensitivity of the current detection in the experimental set-up, which usually ranges from 10^{-5} G_0 to 10^{-9} G_0.

The stretching trace from the BJ measurements reveals several elementary steps, such as the breaking of a metal-metal contact, the sliding of molecules along the electrode, the formation and breaking of a molecular junction. Each step can be distinguished according to the distance between two adjacent

electrodes in the course of opening and closing the nanogap. During the BJ measurements, the current through the nano-junction is much smaller than the current flowing through atomic metal contacts. The shape of individual traces varies considerably due to variations in the structure of the nanojunctions, as well as because of mechanical instabilities of the assembly. Therefore, the determination of the most probable junction properties such as the most probable conductance, plateau lengths, junction formation probability, requires the statistical analysis of hundreds to thousands of individual stretching traces recorded experimentally.[18]

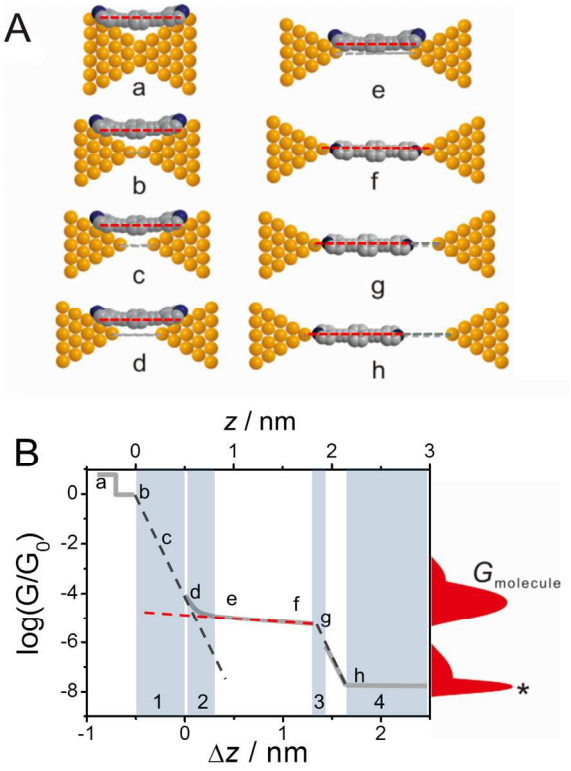

Fig. 3 (A) Scenario of the evolution of a molecular junction during BJ measurements. (B) Simplified schematic representation of a measured conductance trace (solid light gray line) with conductance contributions from direct tunnelling (gray dashed lines) and from the molecule (red dashed line). 1D conductance histogram is depicted in the red color on the right side of the panel B.

The statistical analysis was initially inspired by the metal wire junction studies, in which conductance values of quantized metal junctions show quantized conductance plateau in a linear-scale conductance histogram. Then, this method has been employed in conductance studies of pyridine- and alkanethiol-based molecular systems.[19] To recognize the molecular conductance peaks in linear-scale histogram, in most cases, the data selection was typically required; only individual traces which showed clear molecular conductance plateaus in linear-scale plot were selected for construction of the conductance histogram. Venkataraman *et al.*[20] and González *et al.*[21] presented the conductance histogram in a logarithmic scale, which allowed distinguishing the different conductance features much more easily. The latter also avoided the possible error from the manual data selection and allowed recognition of the junction evolution through various configurations. Additional efforts were made to correlate the conductance and the stretching distance of the nanogap. Part *et al.*[22] proposed a plateau length histogram to reveal the stretched distance distribution of the molecular plateau. Afterwards, a 2D histogram plot was introduced by Martin *et al.*[23] to investigate the overall behavior of the conductance-distance traces upon stretching cycles. Benefitting from these developments, the construction of logarithmic conductance histograms, the plateau length histograms and 2D histograms have been developed as widespread approaches to extract quantitative information from break junction measurements in different research groups with various experimental techniques.

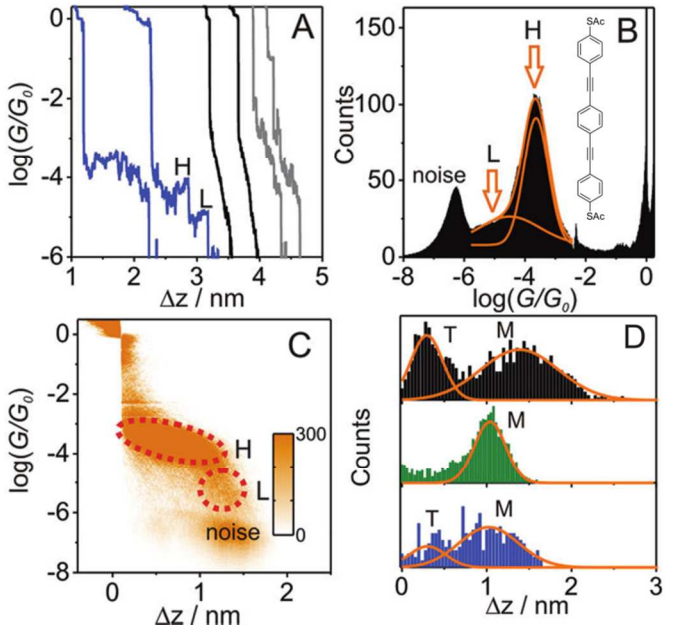

Fig. 4 Statistical analysis of the conductance measurements of OPE3-dithiol (the molecule structure is shown in the panel B) using an STM-BJ (A) Typical conductance distance traces recorded at V_{bias} = 0.1 V. (B) 1D conductance histogram and (C) 2D histogram generated from 2000 individual curves. High and low conductance features are marked by H and L, respectively. (D) Characteristic length distributions for the stretching of molecular junctions, with stretching rates of 145 (black), 58 (green), and 1.45 nm s^{-1} (blue), V_{bias} = 0.10 V. Reprinted with permission from ref. [14] copyright © 2012 American Chemical Society

Fig. 4A, B shows stretching traces recorded for the OPE3-dithiol molecule and the respective 1D conductance histogram in the logarithmic scale. The logarithmic-scale representation enables the direct visualization of experimental data in a wide current (or conductance) range, from several hundred microamps down to a few picoamps, while covering the range of breaking of metal–metal contacts down to the molecular junctions and down to the pure tunneling regime. It also enables a straightforward distinction between molecular junction related features and the background.[14] Moreover, the 2D conductance-distance histogram (Fig. 4C) provides additional valuable information concerning the conductance evolution during the stretching process. The distance axis is aligned with respect to

the atomic contact rupture (zero position). Individual conductance–distance traces obtained in this manner are binned in 2D space and overloaded together.

A meaningful plateau is defined as a series of consecutive data points limited by two "abrupt changes", allowing a certain scatter in the current. These abrupt changes are found by computing the first derivative of the respective single traces. Fig. 4D shows the length distributions of molecular junctions obtained for different stretching rates. Normally, the stretching length is calculated by taking into account the relative zero position and the end of the high conductance feature. In accordance with the assignment and discrimination of direct tunneling (T) and molecular junction (M) contributions, the molecular junction formation probability can be calculated by the relative percentage. Moreover, the most probable plateau length of a molecular junction in a certain conductance range is assigned to the maxima of the relative-displacement distributions Δz^* (Fig. 4C,D). Taking into account the snap-back distance (z_{corr} is ~0.5 nm for Au electrodes[12]), the actual electrode separation z can be estimated: $z=\Delta z+z_{corr}$ (see also Fig. 3B). This actual separation is usually comparable to the molecular length.

In addition, some further data processing approaches have also been employed to analyze the raw data besides the histograms mentioned above. Recently, Makk *et al.*[24] proposed a correlation analysis based on the two-dimensional cross-correlation histogram (2DCH) analysis of the conductance traces. As a complementary approach to the traditional conductance histograms, the 2DCH method provides new information about the relation of different junction configurations that occur during the formation and evolution of single-molecule junctions as well as of metal junctions.

3. Correlation between molecule structure and nanojunction conductance

The comprehensive understanding of charge transport through single molecules and tailored nano-junctions is a fundamental requirement for the design of a functional molecular electric circuit and device. The charge transport in a molecular junction occurs through different junction units: the electrode-molecule interface (junction contact), the molecular backbone and the functional molecular unit (Fig. 5A). In this section, we focus on the correlation between molecule structure and nano-junction conductance through the electrode-molecule interface and molecular backbone. The tuning of the functional unit is discussed in Section 4.

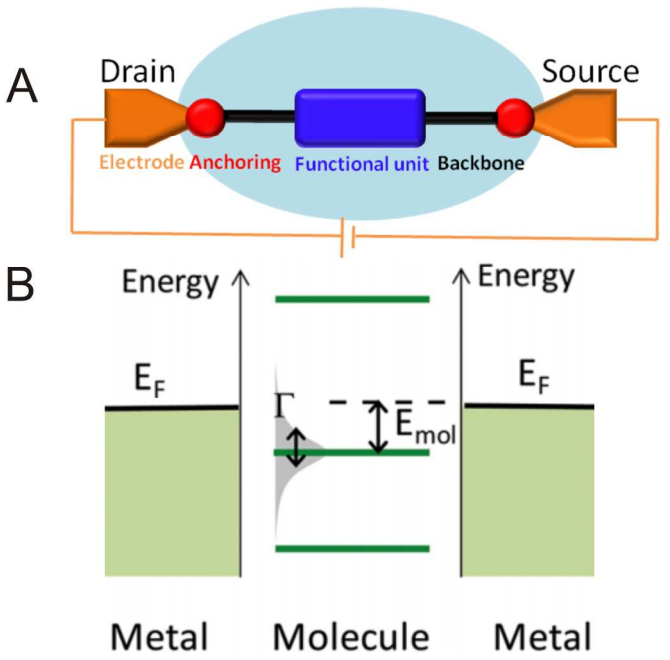

Fig. 5 (A) Schematic of a single molecular junction; (B) Energy level diagram for a single-molecule junction. Here the frontier level is the HOMO. The energy barrier is E_{mol}, and the metal-induced broadening of the HOMO is illustrated, with a broadening width of Γ, reprinted with permission from ref. [25] copyright © 2014 American Chemical Society

3.1. Electrode-molecule interface

The first step of the charge transport through a single-molecular junction is the charge flow through the electrode-molecule interface. When a molecule is coupled with the electrodes, the discrete energy levels of the electrode-molecule interface are shifted and broadened.[26] Therefore, the charge transport through the single molecular junction depends strongly on both the energy barrier E_{mol} (the difference between the Fermi level and molecular orbital offset) and the coupling strength, Γ, between the molecular state and the electrodes.[25] Two major parameters are responsible for controlling the energy level alignment and adjusting the coupling strength, namely the material of the electrodes and the chemical nature of the anchoring groups.

Based on the BJ techniques mentioned above, different metals are used to construct the molecular junction, such as Au, Ag, Pt, and Pd, and non-metal materials such as carbon. For some metals (Ag, Au, Pt and Pd), the Fermi level decreases in the order Ag > Au > Pd > Pt.[27] Recently, Venkataraman's group[28] carried out measurements of single molecular conductance based on Ag electrodes with the STM-BJ technique (Fig. 6A, B). It was demonstrated that the conductance of the amine-terminated oligo-phenyl and alkane molecular junctions with Ag electrodes is lower than that in the case of Au electrodes. Theoretically, for the amine-terminated molecule, the junctions conduct through the HOMO from the Fermi level of the electrode. Therefore, the higher Fermi level of Ag electrodes resulted in a slower charge transport step through the molecule-electrode interface and accordingly in a lower junction

conductance with Ag as electrodes. Ko *et. al.*[19] reported that in the case of $SCN(CH_2)_nNCS$ with a large HOMO-LUMO gap as a model compound, the conductance of the single-molecule junction with three different metal electrodes increased in the order Au < Pd < Pt (Fig. 6C). The junction conductance with Pt or Pd electrodes was found to be about 2.5~3.5-fold superior to that for Au. Such an increase in the conductance cannot be explained by only an effect of different Fermi level of metals. This effect is expected to be insignificant, especially for alkyl chains with a large HOMO-LUMO gap. In the case of Pt and Pd as electrodes, the mixing of π character from the d-orbitals of the Pt and Pd happens, which significantly increases the coupling strength and broaden the energy levels, as shown in figure 5B. The strong energy alignment in the interface and the deceasing of the energy barrier could be responsible for the higher conductance compared to Au contacts with predominant σ-character binding.

Besides the electrode materials, the anchoring groups of the molecule play also an important role in the charge transport process of molecular junctions. Therefore, various anchoring groups have been reported and summarized in the last several years. Employing the STM-BJ technique, Tao's group systematically studied and compared single-molecule conductance of alkanes with -SH (thiol), $-NH_2$ (amine) and -COOH (carboxyl) as anchoring groups.[29] The single-molecule conductance was reported to decrease in the order -SH>$-NH_2$>-COOH. This trend was attributed to different electric coupling efficiencies between the electrode and anchoring groups from the anchoring group side. The measured average length of molecular junctions revealed that the binding strength decreased in the same order Au-S>Au-NH_2>Au-COOH. Since the large HOMO-LUMO gap of the alkyl chains makes the variation of the tunneling barrier height arising from the different anchoring groups negligible, the strength of the electrode-molecule binding (coupling) is responsible for the difference in the conductance. Additionally, Arroyo *et al.* proposed that the deformation of the electrodes caused by the strong binding interaction between anchoring group and electrode should be taken into account when comparing different anchoring groups.[30] The authors concluded that the thiol anchoring group changed the gold electrode dynamics significantly more than amine. Therefore, the amine group could also produce better defined junctions, and could be taken as a model reference. To find an appropriate anchoring group, the molecule-junction conductance, stability, and anchoring strength should be balanced.

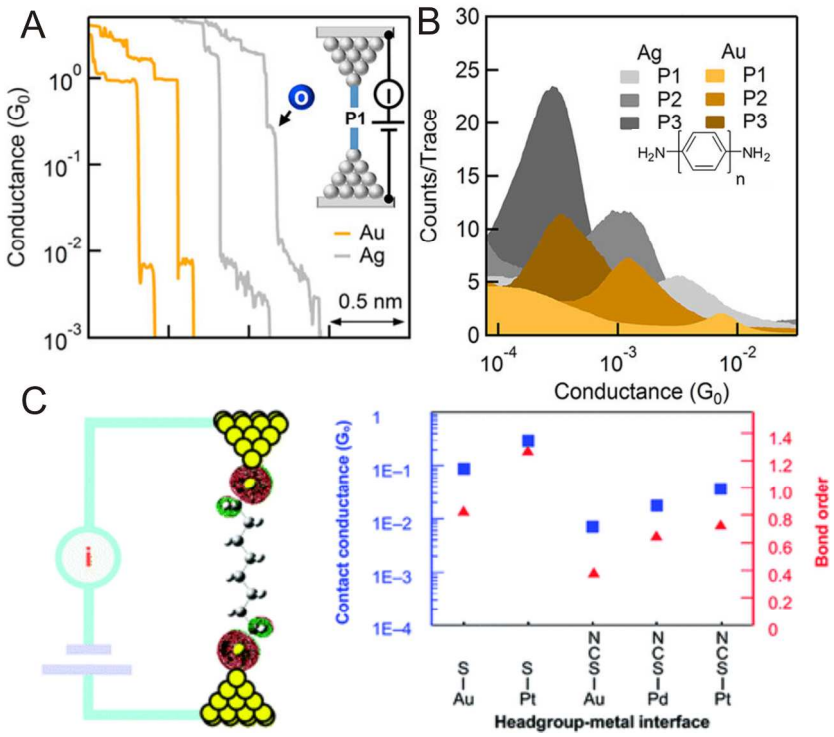

Fig. 6 Conductance studies based on various electrode materials. (A) Sample conductance traces for P1 measured with Au and Ag electrodes. Inset: Illustration of the molecular junction. (B) Log-binned conductance histograms for oligophenyls (P1–P3) generated using 100 bins/decade. P1-P3 correspond to the molecules with 1 to 3 benzene rings, respectively. (C) Correlation of the single-molecule conductance for different electrode materials and binding strength (Mayer bond order) of the molecule–electrode contact. (A) and (B) are reprinted with permission from ref. [28] copyright © 2013 American Chemical Society and (C) from ref. [19] copyright © 2010 American Chemical Society.

Table 1 Summary of the selected anchors and relevant binding properties based on break junction techniques

Molecules	G	Junction formation probability (%)	Charge transport pathway	Ref.
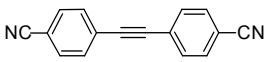	$10^{-4.6}$ G_0	~70	LUMO	13
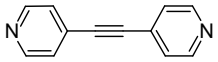	$10^{-3.3}$ G_0	~100	LUMO	13
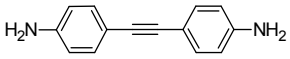	$10^{-3.1}$ G_0	~60	HOMO	13
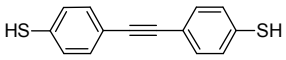	$10^{-2.7}$ G_0	~90	HOMO	13
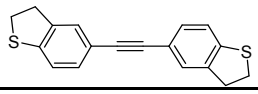	$10^{-2.5}$ G_0	~100	HOMO	15

Recently, benefitting from the latest development of data analysis approaches, our group systematically investigated the single molecular junctions of tolance (diphenylacetylene)-type molecules terminated with -BT (dihydrobenzo[b]thiophene), –SH, -PY (pyridine), -NH_2 and -CN (cyano) using both STM-BJ and MCBJ techniques. [13, 15] As summarized in Table 1, the conductance of the molecular junction increases in the order: -CN << -PY < -NH_2 < -SH < -BT. Also importantly, further analysis on the junction formation probability and the plateau length suggests that the stability of the junction increases in the order: -CN << - NH_2 < -SH < -PY = -BT. Considering both the conductance and the stability of a single molecular junction, -BT exhibits the best anchoring performance among the five groups, with relatively strong binding energy and uniform binding geometry.

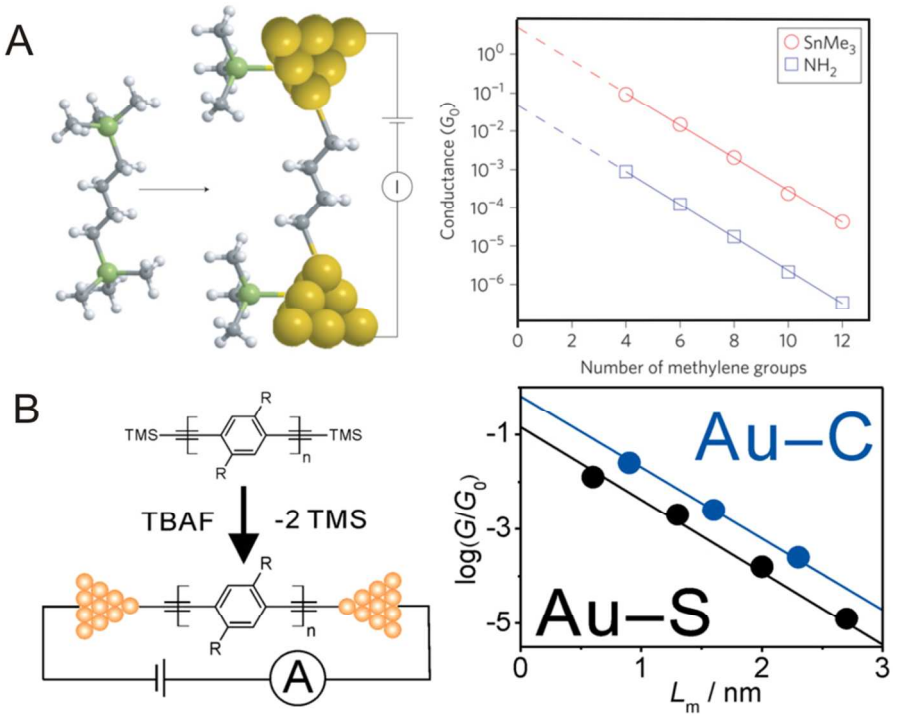

Fig. 7 (A) Junction formation and conductance measurements with 1,4-bis(trimethylstannyl)butane molecules between gold electrodes as Au-C bond (H atoms, white; C atoms, grey; Sn, green) and conductance on a logarithmic scale versus the number of methylene groups in the backbone for $SnMe_3$-terminated alkanes (red) and for diamine-terminated alkanes (blue). Reprinted with permission from ref. [31] copyright © 2011, Rights Managed by Nature Publishing Group (B) Schematics of the Au–C junction formation and plot of the most probable conductance of OPEs versus the molecular length Lm (filled blue circles,). The black circles represent conductance data of the dithiol analogues. Reprinted with permission from ref.[12] copyright © 2013 American Chemical Society

Some attempts were made to develop the covalent gold-carbon attachment. Cheng *et al.*[31] achieved a direct Au-C bond in single molecular junctions for the alkanes and π-conjugated aromatic molecules by the in situ spontaneous cleavage of a trimethyl tin end group ($Sn(CH_3)_3$). As shown in Fig. 7A, the conductance of the molecular junction based on the Au-C σ-bond is about 100 times higher than the analogous molecular junctions with alkanes or aromatic molecules with non-covalent anchoring. Recently, inspired by the protection/deprotection concept in the organic synthesis, our group realized the in situ formation of covalent single-molecule junctions via cleavage of the trimethylsilyl (TMS) protecting group in the MCBJ configuration working in solution.[12] In the presence of a base reagent, the TMS group is cleaved, and the alkynyl moiety attaches to the Au electrode and forms the molecular junction based on the Au-C σ-bond (Fig. 7B). It should be also noted that, for the strong coupled molecular junctions, the influence of the covalent bonding between molecule and electrode cannot be simply assigned to the energy alignment of the interface, because the broadening is so large that partial charge transfer

could happen.[25] Sayed *et al.*[3] determined the work function and molecular orbital onset by ultraviolet photoelectron spectroscopy (UPS) for the carbon/molecule/metal junctions with covalent C-C bonding. They demonstrated that the energy barrier (E_{mol}) of the molecular system with different aromatic structures results in a similar equilibrium value, due to the partial charge transfer between the molecule and bonded electrode (carbon substrate).

3.2. Molecular backbone: length dependence and quantum interference

Besides the molecule-electrode interface, the understanding of charge transport through the molecular backbone is another essential prerequisite towards functionalization of single-molecule devices. The BJ technique provides an ideal testbed to study the correlation between molecular structure and single-molecule conductance. In this section we briefly summarize several key studies.

3.2.1. Length dependence

Two distinct charge transport mechanisms have been predicted theoretically and identified experimentally: coherent transport via tunneling or super-exchange and incoherent thermally activated hopping transport.[32] The tunnelling effect originates from the wave properties of the electrons. Since the electrons pass between two electrodes through a vacuum barrier, the transmission probability T under low bias voltage conditions is given by $T=e^{-\beta d}$, in which d is the barrier width and β is the tunneling constant in units of length^{-1}. In the case of a single molecule acting as tunneling barrier with a certain height, the relevant formula could be modified to molecular conductance $G = Ae^{-\beta L}$, where L is the molecular length. The factor A depends on the electrode-molecule interface. Therefore, an exponential decay of the molecular junction conductance on the molecular length is expected to be observed for the tunneling transport.[32]

Different β values are observed in different molecular wires: i) Non-conjugated systems, such as alkanes.[29] have a rather high tunnelling constant β of around 6-10 nm^{-1}. ii) Highly conjugated systems have quite low tunneling constants (1~4 nm^{-1}) (Fig. 8), e.g. β = 2-3 nm^{-1} for oligoynes, 3.4±0.1 nm^{-1} for the oligophenylene-ethynylenes (OPE), 3.0 nm^{-1} for oligopenyleneimines (OPI), 3.5 nm^{-1} for oligophenylenes (OPP), and 1.7-1.8 nm^{-1} for oligophenylene-vinylenes (OPV).[33] To a certain extent, β illustrates the degree of conjugation of the molecule backbone: the better the conjugation, the lower the β value, which leads to a more conductive junction in a fixed molecular length.

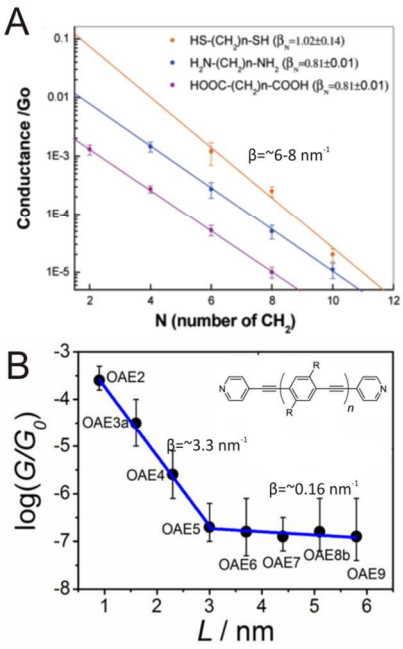

Fig. 8 Length dependence of the conductance of (A) alkane-based molecules and (B) oligo(phenylene-ethynylene) (OPE)-type molecules. Reprinted with permission from (A) ref [29] Copyright © 2006, American Chemical Society and (B) ref. [33] Copyright © 2013, American Chemical Society

In the case of hopping transport, the charge transport involves a nuclear motion, which leads to a temperature dependence as well as to a linear dependence of the conductance on the molecular length. Both of these two charge transport mechanisms exist in the transport through a molecular junction. Much lower β values have been obtained in the case of long molecular systems, where the charge transport is mainly due to the hopping mechanism. One of our recent MCBJ studies demonstrated that the transition between the dominating mechanisms takes place at a molecular length of ~3.0 nm in the pyridine terminated OPE-type molecules with β = ~3.3 nm^{-1} in the tunneling region and β = ~0.16 nm^{-1} in the hopping region (Fig. 8B).[33] Tao's group also carried out STM-BJ conductance measurements of oligophenylene–type molecules.[34] This study also demonstrated a strong length dependence of conductance for the short molecules (with dominating tunneling transport) and temperature dependence of conductance for the long molecules (where hopping dominates). The transition in the charge transport mechanisms occurred in the range of molecular length between 5.2 and 7.3 nm. The variation in the determined transition length of different molecules suggests a joint influence of conjugation, length, and of the selected anchoring group on the charge transport mechanism of specific molecules.

Chemical Soc Rev RSCPublishing

TUTORIAL REVIEW

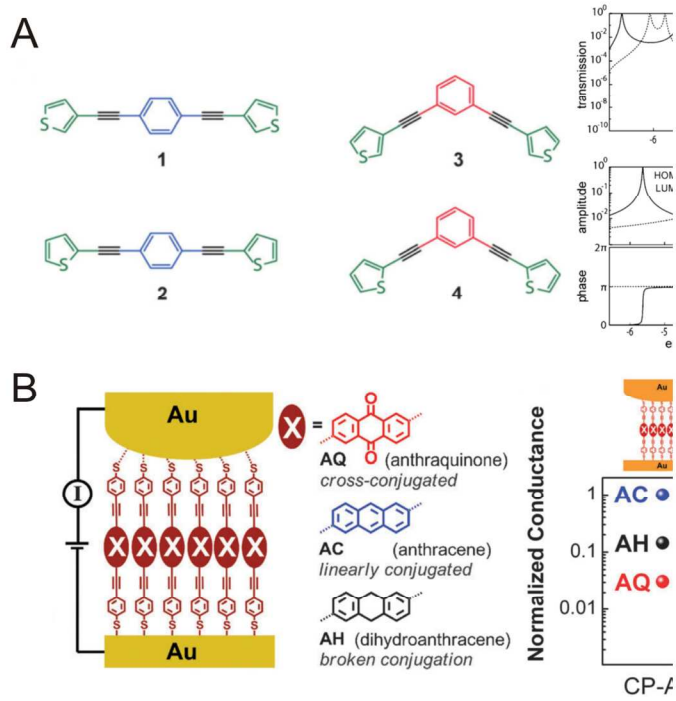

Fig. 9 Quantum inference studies. (A) On the left: Molecular structure of the para- (blue) and meta- (red) coupled benzene rings, coupled to the thienyl anchoring units (green) by ethynyl spacers (black). On the right: (a) calculated transmission through the p-systems of mole-cules **1** (solid line) and **3** (dashed line) in the wide band limit. (b) Amplitude (top) and phase (bottom) of the transmission through the HOMO and LUMO of **1**. (c) Amplitude (top) and phase (bottom) of the transmission through the HOMO and LUMO of 3. Reprinted with permission from ref. [35] Copyright © 2013 WILEY-VCH Verlag GmbH & Co. KGaA, Weinheim (B) Schematic of three molecular wires with different conjugation patterns and in the series of molecules with different conjugation patterns, linearly conjugated AC features the highest values, within statistical error and cross-conjugated AQ the lowest. This trend is the same in CP-AFM, EGaIn, and MCBJ junctions. Reproduced from ref. [36] with the permission of PCCP Owner Societies.

3.2.2 Quantum interference effect

As we discussed in the preceding subchapter, the dominating charge transport mechanisms can be adjusted by varying the molecular length. On the other hand, the wave nature of the electrons transferred through the energy levels provides a possibility to adjust the charge transport pathway by changing the wave functions of the molecule. The quantum interference (QI) which concept is originally from the meso-scale devices, also strongly affects the transmission coefficient of charge transport at single-molecule scale.[37, 38] The QI concept can be used to tune the charge transport at the single-molecule scale by manipulation through the redox process and control of the single-molecule junction conformation.

It was demonstrated that the 1,4-benzenedithiol (*para* configuration) junction shows higher conductance than 1,3-benzenedithiol (*meta* configuration), which was explained by the QI effect in terms of phase shifts of transmission channels or interfering spatial pathways.[39] Arroyo *et al.*[35] studied the QI effect in the single benzene ring with remote anchoring groups (Fig. 9A). Such molecular design reduces an effect of the anchoring groups that can obscure the QI effect. A dramatically higher conductance (by more than 1 order) was observed for *para*-coupled benzene (molecule **1**), compared to meta-coupled benzene (molecule **3**). Based on calculations of the transmission functions, this result was explained by constructive interference for molecule **1** and destructive interference for molecule **3**. The destructive quantum interference was also observed in the cross-conjugated anthquinone unit.[15, 40] Due to the phase difference of π within the HOMO-LUMO gap, the anthquinone-based molecule (AQ) exhibited lower conductance than dihydroanthracene(AH), and almost two orders of magnitude lower conductance than the anthracene-based molecule (AC) as shown in Fig. 9B. The constructive/destructive interference of the electron pathway contributes to the development of a molecular switching device with a significant ON/OFF ratio, suggesting a potential application of efficient single-molecule switches, which will be further discussed in Section 4.

4. Electrochemical gating: toward functionalization

The fabrication of single molecule junctions with the functions of common electronic units, such as rectifiers, switches, or transistors, is a key goal of molecular electronics. Moreover, switching is a main basic function in logic and memory devices. Thus, it is highly attractive to design single-molecule junctions revealing a switching behavior in their conductance between ON and OFF states. The electrochemical gating approach allows tuning the Fermi level of the junction electrodes and to change the redox state of the molecular functional unit (Fig. 5) at room temperature under well-controlled conditions. An electrified solid/liquid interface has also the advantage that two potential differences can be controlled simultaneously: the bias voltage E_{bias} between two working electrodes (source and drain) and the potential drop between each individual working electrode and the reference electrode. [41] The tip and substrate in STM-BJ and two nano-spaced electrodes in MCBJ configurations can serve as source and drain electrodes (Fig. 10). The electrolyte ensures a strong coupling to the applied external field (field strength ~10^9 V m^{-1}, gate thickness ~ 1 nm)[42] and a high mobility of charge carriers (ions). A correlation E(abs)/V = E(SHE)/V + 4.44 V for

aqueous systems,[43] where E(abs) is the absolute energy level and E(SHE) is the electrochemical potential with reference to the standard hydrogen electrode, suggests 100% gating efficiency from the applied electrochemical potential to the energy level shift of the electrodes, in principle.

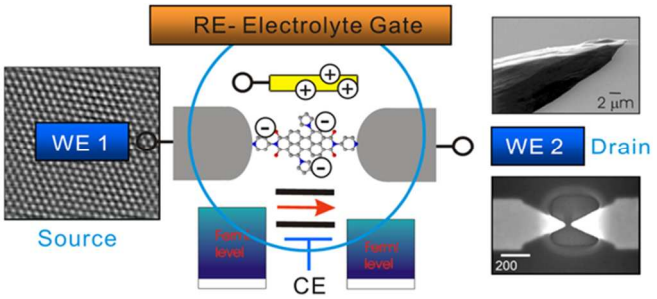

Fig. 10 Working principle of "electrochemical gating" based on the BJ technique. WE1 and WE2 – working, RE – reference, and CE – counter electrodes. Reprinted with permission from ref. [44] Copyright © 2013 WILEY-VCH Verlag GmbH & Co. KGaA, Weinheim

The electrochemical STM-BJ technique (EC-STM-BJ) has been widely used in such studies so far. The STM-BJ requires the insulation of the STM tip by a non-conductive material except for the very end of the tip in order to minimize electrochemical leakage currents and also capacitive current components to no more than ~1 pA. If exceeding the pA range, these unwanted overlapping current components can mask the tunneling current through the nano-junctions. The tip insulation is a rather simple procedure and can be performed in any laboratory. However, in the case of nano-spaced electrodes in the MCBJ configuration the insulation process is rather challenging.[45]

Redox-active molecules represent a particular unique family of switches. They are reduced or oxidized upon the application of an electrochemical gate field in order to achieve the in situ electrochemical gate-controlled charge transport. Recently, some attempts were performed to study the switching behavior of different families of redox-active molecules.[41, 44, 46] However, the achievement of a high ratio between nano-junction conductance in the ON and the OFF states still remains challenging. In particular, a conductance ratio of ~4 was obtained for a pyrrolo-tetrathiafulvalene (pTTF) moiety, attached to gold contacts at both ends through the alkanethiol linker.[41] In this work, a multiple OFF−ON−OFF−ON−OFF conductance switching behavior was observed with ON states at electrode potentials coinciding with the redox peak positions. These redox peaks correspond to two reversible redox processes of the pTTF moiety: formation of a radical cation and a dication. Such a molecular conductance *vs* electrochemical potential relation has been modelled as a sequential two-step charge-transfer process with full or partial vibrational relaxation (Kuznetsov-Ulstrup model).[42]

A nearly one-order magnitude conductance ratio was experimentally found for the anthraquinone /hydroanthraquinone (AQ/H_2AQ), redox couple (Fig. 11).[46] The AQ group was embedded into a rigid norbornylogous (NB) unit bearing two pairs of thiol groups at each end serving as linkers to the electrodes, Based on experimental results[46] and computational predictions, the switching mechanism was explained by the presence of destructive quantum interference between various conductance channels in the cross-conjugated AQ (OFF state), which is absent in the linear conjugated H_2AQ (ON state), Furthermore, this work demonstrated that potential windows of ON and OFF states can be tuned by the pH value of an electrolyte solution (Fig. 11).

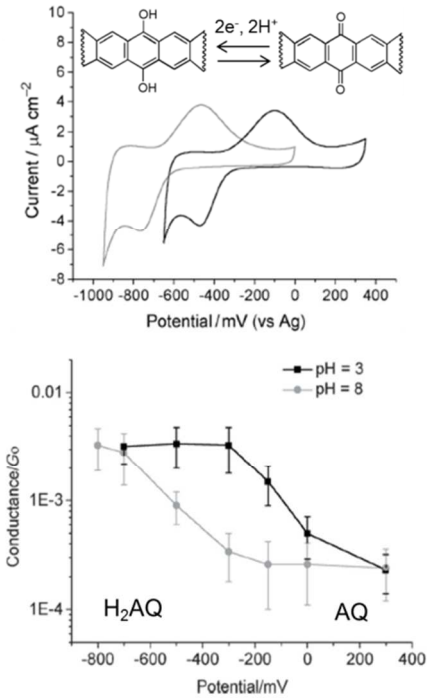

Fig. 11 Cyclic voltammetry of redox-active 5AQ5 SAM on Au(111) electrode in the electrolyte solutions of pH 3 (black line) and pH 8 (grey line) and respective evolution of the conductance of 5AQ5 with an electrochemical potential. Reprinted with permission from Ref. [46] Copyright © 2012 WILEY-VCH Verlag GmbH & Co. KGaA, Weinheim

Li et al. attempted to improve the electrochemical switching behavior of redox-active benzodifuran-based molecules (BDF) by selection of optimal anchoring groups.[47] The use of the carbodithioate (-CS_2^-) anchoring group instead of thiolate resulted in a dramatically increased molecular junction conductance and switching efficiency. The ON/OFF ratio was claimed to be 8 for carbodithioate-BDF.

Besides the redox active molecules, Capozzi et al.[48] reported a tunable charge transport in single-molecule junction via electrolytic gating based on one non-redox active molecular system. They demonstrated that for the molecule 1,2-bis(4, 4-dimethylthiochroman-6-yl)ethylene (**1**), conducting through the HOMO, the conductance of a single-molecule junction decreased with increasing gate potential (Fig. 12, left panel). The opposite trend was observed for the molecular system 1,2-bis(4-pyridyl)ethylene (**2**) that conducts through the LUMO, (Fig. 12, right panel). Theoretically, the increase of the gate potential drives the LUMO in the molecular orbitals closer to the Fermi level of the electrode and pushes the HOMO further

away, resulting in an enhanced charge transport for the LUMO transport single-molecule junction. Baghernejad et al.[49] employed an STM-BJ technique under electrochemical condition to study charge transport through 4, 4-bipyridine single-molecule junctions. This work demonstrates that electrochemical gating in aqueous electrolyte provides a viable platform for tuning the charge transport through single-molecule junctions with 100% gating efficiency between the electrode potential and the alignment of frontier molecular levels.

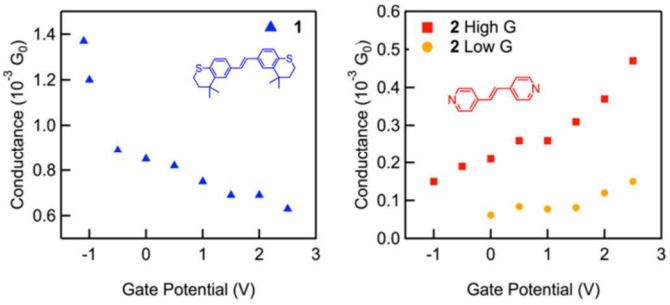

Fig. 12 Peak conductance values versus applied gate potential for molecules **1** and **2**, respectively. The molecule structures are depicted in the respective plots. The molecule **2** has two conductance features: high (red squares) and low (orange circles) conductance. Reprinted with permission from ref. [48] Copyright © 2014, American Chemical Society

Similar effect is also observed in redox-inactive potential regime of the redox-active molecules. A recent study of anthraquinone-based molecules with the pyridine anchors showed that the single-molecule conductance could be controlled via both redox switching and Fermi level tuning varying electrode potential. In redox-inactive potential region, the effect of the gating is to shift the Fermi level relative to the molecular resonances leading to a modest change in the conductance. The further shift of electrode potential led a large and reversible jumps of the conductance due to the change in the molecular redox state, which was accompanied with changes from linear (in the reduced state) to cross conjugation (in the oxidized state). This work also suggest that electrochemical gating of single-molecule junction can be modeled using relatively simple computational models via conversion of potential to energy scale.[50]

5. Conclusion and perspective

In this review, we highlighted the recent developments on charge transport through single-molecule junction studies at the solid-liquid interface. Based on the well-established break junction technique and the corresponding developed data analysis, single-molecule conductance can be measured with remarkably improved reproducibility. The studies of the correlation between single-molecule conductance and molecular structure provide the guideline for future organic molecular design and synthesis for molecular electronics.

In clear distinction from conventional electronics, the functions of molecular components are achieved by inducing changes in the molecular structure and/or by tuning the energy levels of the molecular junction. For this purpose, the electrochemical gating approach offers a highly promising platform for the construction and investigation of electrochemically controllable switches or field effect transistors (FETs) based on both redox-active or redox-inactive molecular systems.

As a perspective, there are series of experimental efforts to incorporate *in situ* spectroscopy, for instance Raman spectroscopy, into single-molecule conductance measurements using break junction techniques. These developments will allow monitoring the charge transport and molecular structure changes simultaneously, which is expected to be a perfect testbed for future molecular electronics studies.

Acknowledgements

We acknowledge the funding support by the Swiss National Science Foundation (Grant No. 200020-144471), EPSRC and by EC FP7 ITN "MOLESCO". A.R. acknowledges FP7 project ACMOL (No 618082). We also highly appreciate H. Siegenthaler and S. Decurtins for helpful discussions and proof reading.

Reference

1. J. C. Cuevas and E. Scheer, in *Molecular Electronics: An Introduction to Theory and Experiment*, World Scientific, Singapore, 2010, vol. 1.
2. R. C. Chiechi, E. A. Weiss, M. D. Dickey and G. M. Whitesides, *Angew. Chem. Int. Ed.*, 2008, **47**, 142-144.
3. S. Y. Sayed, J. A. Fereiro, H. Yan, R. L. McCreery and A. J. Bergren, *Proc. Natl. Acad. Sci.*, 2012, **109**, 11498-11503.
4. B. Q. Xu and N. J. J. Tao, *Science*, 2003, **301**, 1221-1223.
5. C. Li, I. Pobelov, T. Wandlowski, A. Bagrets, A. Arnold and F. Evers, *J. Am. Chem. Soc.*, 2007, **130**, 318-326.
6. C. W. Wolfgang Haiss, Iain Grace, Andrei S. Batsanov, David J. Schiffrin, Simon J. Higgins, Martin R. Bryce, Colin J. Lambert & Richard J. Nichols, *Nat. Mater.*, 2006, **5**, 995 - 1002.
7. Huang, Xu, Chen, M. D. Ventra and Tao, *Nano Lett.*, 2006, **6**, 1240-1244.
8. C. J. Muller, J. M. van Ruitenbeek and L. J. de Jongh, *Phys. Rev. Lett.*, 1992, **69**, 140-143.
9. M. A. Reed, C. Zhou, C. J. Muller, T. P. Burgin and J. M. Tour, *Science*, 1997, **278**, 252-254.
10. A. M. Christian, M. v. R. Jan and S. J. v. d. Z. Herre, *Nanotech.*, 2010, **21**, 265201.
11. T. Konishi, M. Kiguchi, M. Takase, F. Nagasawa, H. Nabika, K. Ikeda, K. Uosaki, K. Ueno, H. Misawa and K. Murakoshi, *J. Am. Chem. Soc.*, 2013, **135**, 1009-1014.
12. W. Hong, H. Li, S.-X. Liu, Y. Fu, J. Li, V. Kaliginedi, S. Decurtins and T. Wandlowski, *J. Am. Chem. Soc.*, 2012, **134**, 19425-19431.
13. W. Hong, D. Z. Manrique, P. Moreno-García, M. Gulcur, A. Mishchenko, C. J. Lambert, M. R. Bryce and T. Wandlowski, *J. Am. Chem. Soc.*, 2011, **134**, 2292-2304.
14. V. Kaliginedi, P. Moreno-Garcia, H. Valkenier, W. Hong, V. M. Garcia-Suarez, P. Buiter, J. L. H. Otten, J. C. Hummelen,

C. J. Lambert and T. Wandlowski, *J. Am. Chem. Soc.*, **134**, 5262-5275.
15. P. Moreno-García, M. Gulcur, D. Z. Manrique, T. Pope, W. Hong, V. Kaliginedi, C. Huang, A. S. Batsanov, M. R. Bryce, C. Lambert and T. Wandlowski, *J. Am. Chem. Soc.*, 2013, **135**, 12228-12240.
16. C. R. Parker, E. Leary, R. Frisenda, Z. Wei, K. S. Jennum, E. Glibstrup, P. B. Abrahamsen, M. Santella, M. A. Christensen, E. A. Della Pia, T. Li, M. T. Gonzalez, X. Jiang, T. J. Morsing, G. Rubio-Bollinger, B. W. Laursen, K. Nørgaard, H. van der Zant, N. Agrait and M. B. Nielsen, *J. Am. Chem. Soc.*, 2014, **136**, 16497-16507.
17. B. Gotsmann, H. Riel and E. Lörtscher, *Phys. Rev. B*, 2011, **84**, 205408.
18. J. Ulrich, D. Esrail, W. Pontius, L. Venkataraman, D. Millar and L. H. Doerrer, *J. Phys. Chem. B*, 2006, **110**, 2462-2466.
19. C.-H. Ko, M.-J. Huang, M.-D. Fu and C.-h. Chen, *J. Am. Chem. Soc.*, 2009, **132**, 756-764.
20. L. Venkataraman, J. E. Klare, C. Nuckolls, M. S. Hybertsen and M. L. Steigerwald, *Nature*, 2006, **442**, 904-907.
21. M. T. González, S. Wu, R. Huber, S. J. van der Molen, C. Schönenberger and M. Calame, *Nano Lett.*, 2006, **6**, 2238-2242.
22. Y. S. Park, A. C. Whalley, M. Kamenetska, M. L. Steigerwald, M. S. Hybertsen, C. Nuckolls and L. Venkataraman, *J. Am. Chem. Soc.*, 2007, **129**, 15768-15769.
23. C. A. Martin, D. Ding, J. K. Sørensen, T. Bjørnholm, J. M. van Ruitenbeek and H. S. J. van der Zant, *J. Am. Chem. Soc.*, 2008, **130**, 13198-13199.
24. P. Makk, D. Tomaszewski, J. Martinek, Z. Balogh, S. Csonka, M. Wawrzyniak, M. Frei, L. Venkataraman and A. Halbritter, *ACS Nano*, 2012, **6**, 3411-3423.
25. S. Y. Quek and K. H. Khoo, *Acc. Chem. Res.*, 2014, **47**, 3250-3257.
26. D. Cahen and A. Kahn, *Adv. Mater.*, 2003, **15**, 271-277.
27. D. Xiang, H. Jeong, T. Lee and D. Mayer, *Adv. Mater.*, 2013, **25**, 4845-4867.
28. T. Kim, H. Vázquez, M. S. Hybertsen and L. Venkataraman, *Nano Lett.*, 2013, **13**, 3358-3364.
29. F. Chen, X. Li, J. Hihath, Z. Huang and N. Tao, *J. Am. Chem. Soc.*, 2006, **128**, 15874-15881.
30. C. R. Arroyo, E. Leary, A. Castellanos-Gómez, G. Rubio-Bollinger, M. T. González and N. Agraït, *J. Am. Chem. Soc.*, 2011, **133**, 14313-14319.
31. Z.-L. Cheng, R. S. , H. V. , J. R. W. , S. Schneebeli, W. C. , M. S. H. , R. Breslow and L. Venkataraman, *Nat. Nanotechnol.*, 2011, **6**, 353-357.
32. S. H. Choi, B. Kim and C. D. Frisbie, *Science*, 2008, **320**, 1482-1486.
33. X. Zhao, C. Huang, M. Gulcur, A. S. Batsanov, M. Baghernejad, W. Hong, M. R. Bryce and T. Wandlowski, *Chem. Mater.*, 2013, **25**, 4340-4347.
34. T. Hines, I. Diez-Perez, J. Hihath, H. M. Liu, Z. S. Wang, J. W. Zhao, G. Zhou, K. Muellen and N. J. Tao, *J. Am. Chem. Soc.*, 2010, **132**, 11658-11664.
35. C. R. Arroyo, S. Tarkuc, R. Frisenda, J. S. Seldenthuis, C. H. M. Woerde, R. Eelkema, F. C. Grozema and H. S. J. van der Zant, *Angew. Chem. Int. Ed.*, 2013, **52**, 3152-3155.
36. H. Valkenier, C. M. Guedon, T. Markussen, K. S. Thygesen, S. J. van der Molen and J. C. Hummelen, *Phys. Chem. Chem. Phys.*, 2014, **16**, 653-662.
37. T. Markussen, R. Stadler and K. S. Thygesen, *Nano Lett.*, 2010, **10**, 4260-4265.
38. C. J. Lambert, *Chem. Soc. Rev.*, 2015, 10.1039/C1034CS00203B.
39. M. Kiguchi, H. Nakamura, Y. Takahashi, T. Takahashi and T. Ohto, *J. Phy. Chem. C*, 2010, **114**, 22254-22261.
40. H. V. Constant M. Guédon, Troels Markussen, Kristian S. Thygesen, Jan C. Hummelen, Sense Jan van der Molen, *Nat. Nanotechnol.*, 2012, **7**, 305-309.
41. N. J. Kay, S. J. Higgins, J. O. Jeppesen, E. Leary, J. Lycoops, J. Ulstrup and R. J. Nichols, *J. Am. Chem. Soc.*, 2012, **134**, 16817-16826.
42. J. Zhang, A. M. Kuznetsov, I. G. Medvedev, Q. Chi, T. Albrecht, P. S. Jensen and J. Ulstrup, *Chem. Rev.*, 2008, **108**, 2737-2791.
43. S. Trasatti, *Pure Appl. Chem.*, 1986, **58**, 955-966.
44. C. Li, V. Stepanenko, M.-J. Lin, W. Hong, F. Wuerthner and T. Wandlowski, *Phys. Status Solidi B*, 2013, **250**, 2458-2467.
45. Y. Yang, J.-Y. Liu, Z.-B. Chen, J.-H. Tian, X. Jin, B. Liu, X. Li, Z.-Z. Luo, M. Lu, F.-Z. Yang, N. Tao and Z.-Q. Tian, *Nanotech.*, 2011, **22**.
46. N. ACS NanoDarwish, I. Diez-Perez, P. Da Silva, N. Tao, J. J. Gooding and M. N. Paddon-Row, *Angew. Chem. Int. Ed.*, 2012, **51**, 3203-3206.
47. Z. Li, H. Li, S. Chen, T. Froehlich, C. Yi, C. Schönenberger, M. Calame, S. Decurtins, S.-X. Liu and E. Borguet, *J. Am. Chem. Soc.*, 2014, **136**, 8867-8870.
48. B. Capozzi, Q. Chen, P. Darancet, M. Kotiuga, M. Buzzeo, J. B. Neaton, C. Nuckolls and L. Venkataraman, *Nano Lett.*, 2014, **14**, 1400-1404.
49. M. Baghernejad, D. Z. Manrique, C. Li, T. Pope, U. Zhumaev, I. Pobelov, P. Moreno-Garcia, V. Kaliginedi, C. Huang, W. Hong, C. Lambert and T. Wandlowski, *Chem. Comm.*, 2014, **50**, 15975-15978.
50. M. Baghernejad, X. Zhao, K. B. Ørnsø, M. Füeg, P. MorenoGarcía, A. V. Rudnev, V. Kaliginedi, S. Vesztergom, C. Huang, W. Hong, P. Broekmann, T. Wandlowski, K. S. Thygesen, M. R. and M. R. Bryce, *J. Am. Chem. Soc.*, 2014, 10.1021/ja510335z.

